Quantum Hall effect in Bernal stacked and twisted bilayer graphene grown on Cu by chemical vapor deposition

Babak Fallahazad,[1] Yufeng Hao,[2] Kayoung Lee,[1] Seyoung Kim,[1] R. S. Ruoff,[2] and E. Tutuc[1,*]

[1]*Microelectronics Research Center, The University of Texas at Austin, Austin, Texas 78758, USA*
[2]*Department of Mechanical Engineering and the Materials Science and Engineering Program,*
The University of Texas, Austin, Texas 78712, USA

We examine the quantum Hall effect in bilayer graphene grown on Cu substrates by chemical vapor deposition. Spatially resolved Raman spectroscopy suggests a mixture of Bernal (A-B) stacked and rotationally faulted (twisted) domains. Magnetotransport measurements performed on bilayer domains with a wide 2D band reveal quantum Hall states (QHSs) at filling factors $\nu = 4, 8, 12$, consistent with a Bernal stacked bilayer, while magnetotransport measurements in bilayer domains defined by a narrow 2D band show a superposition of QHSs of two independent monolayers. The analysis of the Shubnikov–de Haas oscillations measured in twisted graphene bilayers provides the carrier density in each layer as a function of the gate bias and the interlayer capacitance.

PACS number(s): 73.22.Pr, 73.43.−f, 68.35.bp

Bilayer graphene consisting of two closely spaced graphene monolayers is an interesting electron system. If the two graphene monolayers forming the bilayer are Bernal stacked, the system possesses a tunable energy band gap,[1–4] which renders it attractive for electronic and optoelectronic applications. While electron transport in natural bilayer graphene has been explored to a large extent, much less is known about the transport properties of *grown* graphene bilayers. Recent studies have reported the growth of bilayer graphene on SiC and metal substrates by chemical vapor deposition (CVD). Bilayer graphene grown on SiC substrates has been shown to be Bernal stacked when grown on the Si-face,[5,6] and rotationally twisted when grown on the C-face.[7] While several recent studies suggest the growth of Bernal stacked bilayer on metal substrates based on Raman spectroscopy,[8–11] evidence of stacking from electron transport data in grown bilayer graphene has been scant. It is therefore interesting to probe the electronic properties of CVD-grown graphene bilayers, which in turn can shed light on the growth mechanism and help assess its potential for applications. Here we provide a systematic investigation of the quantum Hall effect in bilayer graphene grown on Cu substrates by chemical vapor deposition. Our data show that such bilayers consist of a *mixture* of domains which are either Bernal stacked or are rotationally faulted ("twisted bilayer").

The graphene samples studied here are grown on a 25-μm-thick Cu foil at a temperature of 1035 °C by CVD, using a mixture of methane and hydrogen at partial pressures of 0.02 and 0.03 mbar, respectively. After the growth, the graphene film on one side of the Cu foil is coated with poly(methyl methacrylate) (PMMA) and placed in an aqueous solution of ammonia persulfate [$(NH_4)_2S_2O_8$] to dissolve the Cu on the unprotected side. The PMMA film that carries the graphene flake is rinsed several times with de-ionized water to minimize the chemical contamination, and then transferred onto a silicon substrate covered with 285-nm-thick thermally grown SiO_2. After the transfer the sample is allowed to dry, and the PMMA is dissolved in acetone.

Figure 1(a) shows an optical micrograph of the graphene film transferred on the SiO_2 substrate, indicating the presence of monolayer, bilayer, and trilayer regions. To probe the number of graphene layers, and obtain an initial assessment of the layer stacking, the sample is characterized by Raman spectroscopy acquired using a 488-nm excitation wavelength, 300-nm spot size, and a power lower than 0.1 mW. Figure 1(b) presents a representative mapping of the Raman 2D band full width at half maximum (FWHM) acquired over a 30×30 μm^2 area. These data reveal the presence of distinct domains on the bilayer area with either a narrow 2D band, with FWHM values between 27 and 33 cm^{-1}, or a wide 2D band, with FWHM values between 45 and 54 cm^{-1}. By comparison the Raman 2D FWHM measured in monolayer graphene is 28–30 cm^{-1}, while in Bernal (A-B) stacked bilayer graphene the 2D band is wider.[12–16] Figure 1(b) data therefore suggest that the bilayer domains with a narrow 2D band consist of two graphene monolayers which are rotationally faulted (twisted bilayer), while the domains characterized by a wider 2D band consist of two Bernal stacked monolayers. We note the two types of bilayer domains of Fig. 1(b) show no obvious differences in optical contrast. Figure 1(c) shows samples of Raman spectra acquired on the same sample of Fig. 1(b), at different positions on the monolayer, the twisted bilayer, and the Bernal stacked bilayer regions, as indicated. The 2D FWHM of these Raman spectra are 28, 30, and 50 cm^{-1}, respectively. The 2D band intensity (I_{2D}) is larger than the G band intensity (I_G) on the monolayer and bilayer domains with a narrow 2D band, an observation which agrees with Raman spectroscopy results for exfoliated graphene.[12,13] In contrast, the bilayer domain with a wide 2D band shows an I_{2D}/I_G ratio lower than 1. The D band, located at a Raman shift of 1350 cm^{-1}, is either absent or very weak, indicating that the defect density is low.

Figure 1(d) shows a histogram of the 2D band FWHM values acquired over a 15×20 μm^2 bilayer graphene grain characterized by a wide 2D band. The data points range between 45 and 65 cm^{-1}, with a maximum at 53 cm^{-1}. Figure 1(e) presents a typical spectrum of the 2D band selected from the bilayer graphene region with a wide 2D band. Figure 1(e) data could not be fitted well using a single
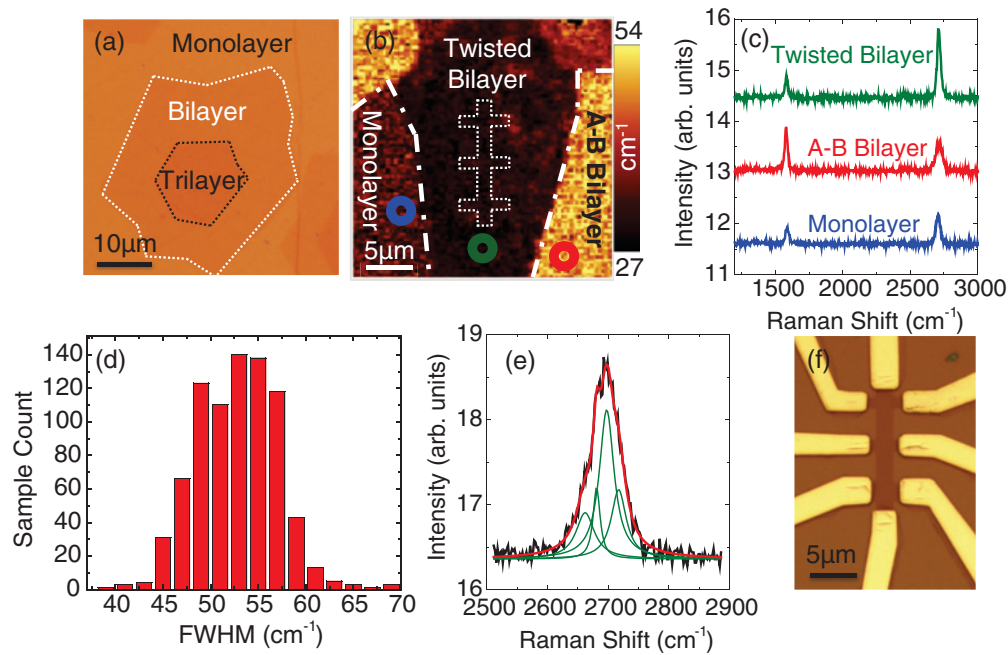
FIG. 1. (Color) (a) Optical micrograph of a multilayer graphene sample after transfer onto a 285-nm-thick SiO$_2$/Si substrate. The dashed lines delineate monolayer, bilayer, and trilayer regions. (b) 2D FWHM spatial map reveals the bilayer is a mixture of domains with either a wide (45–54 cm^{-1}) or narrow (27–33 cm^{-1}) 2D band. The dotted line marks a Hall bar subsequently fabricated to probe electron transport in individual bilayer regions. (c) Raman spectra acquired at three different positions, as marked in (b), show the G ($\simeq$1580 cm^{-1}) and 2D ($\simeq$2700 cm^{-1}) bands. (d) Histogram of the 2D band FWHM on a bilayer domain with a wide 2D band. The average 2D FWHM is 53 $\pm$ 2 cm^{-1}. (e) Example of a 2D band spectrum (black line) acquired on a Bernal stacked bilayer domain. A fit (red) using four Lorentzian functions (green) provides a very good match to the experimental data. (f) Optical micrograph of a back-gated Hall bar fabricated on bilayer graphene.

Lorentzian, but an excellent fit is obtained using four Lorentzian functions. The combined data of Figs. 1(b)–1(e) therefore suggest that bilayer domains with a narrow 2D band consist of twisted graphene monolayers, while the bilayer domains with a wide 2D band are two Bernal stacked monolayers. We next focus on the magnetotransport in these two types of bilayers.

After the graphene is characterized by Raman spectroscopy, we fabricate back-gated Hall bar devices on selected bilayer domains with a uniform 2D peak FWHM, which is either narrow (27–33 cm^{-1}) or wide (45–65 cm^{-1}). The active region of the Hall bar is defined by electron-beam (e-beam) lithography and isolated from the rest of the film using oxygen plasma etching. Metal (Ni) contacts are defined by a second e-beam lithography, metal deposition, and liftoff [Fig. 1(f)]. The carrier mobility (μ) of each sample is determined from the four-point conductivity (σ) dependence on back-gate bias (V_{BG}), $\mu = 1/C_{BG} \times d\sigma/dV_{BG}$; C_{BG} is the back-gate capacitance per unit area. For the samples examined in this study C_{BG} lies in the range $12.5 - 14.4$ nF cm^{-2}, values measured on metal pads deposited in proximity to the Hall bars, and by Hall measurements. The extracted mobility of the Bernal stacked bilayer graphene devices range between 700 and 1800 cm^2 V^{-1} s^{-1} at room temperature and between 1800 and 2200 cm^2 V^{-1} s^{-1} at 0.3 K. The twisted bilayers exhibit mobility values between 3400 and 3700 cm^2 V^{-1} s^{-1} at room temperature and between 5300 and 7600 cm^2 V^{-1} s^{-1} at 0.3 K. The higher mobility in twisted bilayers in comparison to Bernal stacked bilayers can be explained by differences in

their band structure, which forbid electron backscattering in monolayer graphene, and hence in a twisted bilayer, but allow backscattering in Bernal stacked bilyers.[17]

To establish the layer stacking of the CVD-grown graphene bilayers and explore their electronic properties, in the following we discuss the quantum Hall effect in this system. Magnetotransport measurements were carried out in perpendicular magnetic fields (B) up to 31 T, using a pumped ^{3}He refrigerator with a base temperature $T = 0.3$ K, and small signal, low frequency lock-in techniques. Figure 2(a) shows the longitudinal (ρ_{xx}) and Hall resistivity (ρ_{xy}) as a function of V_{BG} measured at a perpendicular magnetic field $B = 25$ T and $T = 0.3$ K in a graphene bilayer that displays a Raman signature consistent with Bernal stacking, i.e., a wide 2D band. The data show clear quantum Hall states (QHSs), marked by vanishing ρ_{xx} and quantized ρ_{xy} at filling factors $\nu = \pm 4$ and $\nu = -8$. The filling factors are determined from the ρ_{xy} plateau values, which are equal to $h/\nu e^2$; h is Planck's constant and e the electron charge. Alternatively, the filling factor can be calculated using $\nu = nh/eB$, where n is the total carrier density calculated by $n = C_{BG}(V_{BG} - V_D)/e$; V_D is the gate bias at the charge neutrality (Dirac) point.

Figure 2(b) shows the ρ_{xx} vs ν measured in the same sample at different B values, and at $T = 0.3$ K. The data show the emergence of QHSs at integer filling factors that are multiples of four, i.e., $\nu = \pm 4, -8, -12$, thanks to the fourfold degeneracy of each Landau level (LL) associated with the spin and valley degrees of freedom.[18] The QHS filling factors of Figs. 2(a) and 2(b) are consistent with the expected
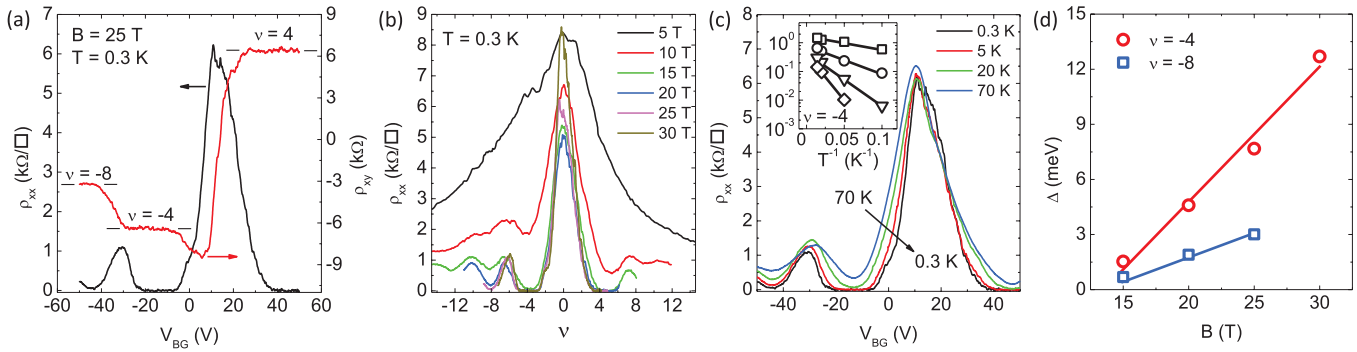
FIG. 2. (Color) (a) ρ_{xx} and ρ_{xy} vs V_{BG}, measured at $B = 25$ T, and $T = 0.3$ K. The data shows QHSs, marked by vanishing ρ_{xx} and quantized ρ_{xy}, at filling factors $\nu = \pm 4$ and $\nu = -8$. (b) ρ_{xx} vs ν measured at $T = 0.3$ K, and at different B-field values, illustrating the emergence of QHSs at integer filling factors that are multiples of four with increasing the B field. (c) ρ_{xx} vs V_{BG} measured at different temperatures, and at $B = 25$ T. Inset: ρ_{xx} vs T^{-1} at $\nu = -4$ on a log-lin scale, measured at $B = 15$ T ($\square$), 20 T ($\circ$), 25 T ($\triangledown$), 30 T ($\diamond$). (d) Δ vs B, for $\nu = -4$ and $\nu = -8$ QHSs. The solid lines are guide to the eye.

values in natural bilayer graphene,[18,19] in effect fingerprinting a Bernal stacked bilayer. Figure 2(c) shows ρ_{xx} vs V_{BG} measured at $B = 25$ T, and at different temperatures. Although the $\nu = \pm 4, -8$ QHSs weaken with increasing T, these QHSs remain clearly visible at the highest temperature, $T = 70$ K. The inset of Fig. 2(c) shows the Arrhenius plot of ρ_{xx} measured at $\nu = -4$, and at $B = 15, 20, 25$, and 30 T. These data follow a thermally activated behavior, $\rho_{xx} \propto e^{-\Delta/(2k_B T)}$, where Δ is the energy gap and k_B is Boltzmann's constant. Figure 2(d) shows the extracted $\nu = -4, -8$ QHS energy gaps versus B. The data follow a linear dependence of Δ as a function of B, with the Δ values approaching 0 at $B \simeq 13$ T. The QHS energy gaps of Fig. 2(d) are considerably smaller than theoretical values.[20] For example, the theoretically expected energy gap of $\nu = -4$ at $B = 30$ T is 108 meV, a value roughly eight times larger than the experimental value. The $\nu = -4$ and $\nu = -8$ QHS energy gaps probed in CVD-grown bilayer graphene are also approximately fivefold smaller than values typically measured in exfoliated bilayer graphene on SiO$_2$ substrates.[21,22]

We now turn to the magnetotransport properties of the twisted bilayer graphene samples, fabricated on bilayer graphene domains with a narrow Raman 2D band. Figure 3(a) shows an example of ρ_{xx} and ρ_{xy} vs B data, measured in a

twisted bilayer device at $V_{BG} = -40$ V, corresponding to $n = -8.4 \times 10^{12}$ cm^{-2}, and at $T = 0.3$ K; the sample mobility is $\mu = 7400$ cm^2 V^{-1} s^{-1}. These data possess several noteworthy features. First, the ρ_{xx} vs B data display Shubnikov–de Haas (SdH) oscillations present down to magnetic fields as low as $B \simeq 3$ T, which contrast Fig. 2(b) data, where QHSs are not visible at B fields lower than 10 T. This observation can be explained by the larger monolayer graphene LL energies in comparison to bilayer graphene. Moreover, the ρ_{xx} vs B data do not follow a QHS sequence which can be readily attributed to either a monolayer ($\nu = \pm 2, 6, 10, \ldots$) or bilayer ($\nu = \pm 4, 8, 12, \ldots$), and instead shows a beating pattern similar to the QHS superposition of a multisubband system, consistent with parallel electron transport in two independent graphene monolayers.

To determine the subband (layer) density in a twisted bilayer, we examined the Fourier transform (FT) of ρ_{xx} vs B^{-1} data, calculated by first replotting the ρ_{xx} vs B data, subtracting a linear fit background to center the ρ_{xx} vs B^{-1} data around zero, and then applying a fast Fourier transform algorithm. Figure 3(b) shows the FT amplitude versus frequency corresponding to Fig. 3(a) data. These data show two prominent peaks, which yield the two layer densities,
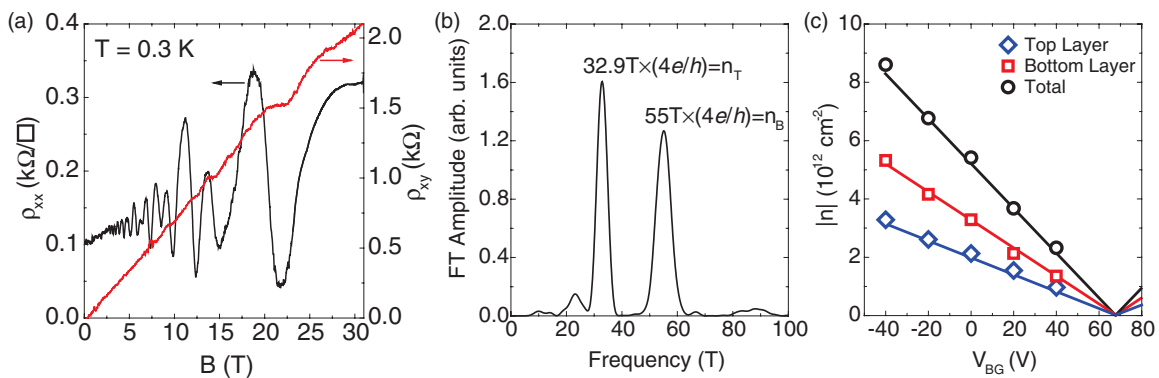

FIG. 3. (Color) (a) ρ_{xx} and ρ_{xy} vs B measured at $n = -8.4 \times 10^{12}$ cm^{-2} and at $T = 0.3$ K. The SdH oscillations stem from a QHSs superposition of the two decoupled graphene monolayers. (b) Fourier transform of ρ_{xx} vs B^{-1} data. The two peaks represent the layer densities, up to a factor $4e/h$. (c) Top layer, bottom layer, and total carrier densities of the twisted bilayer graphene vs V_{BG}. The symbols (lines) represent experimental data (calculations).
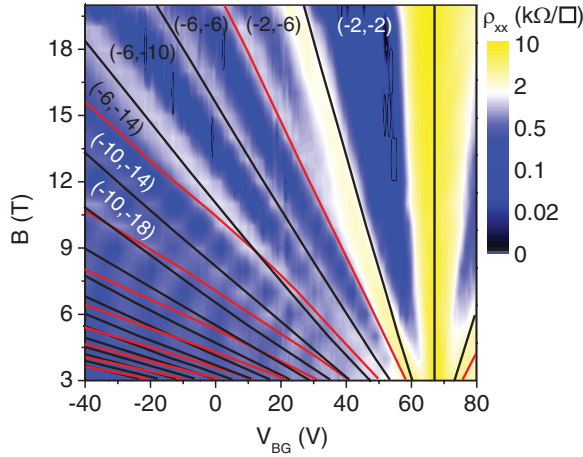
FIG. 4. (Color) Twisted bilayer ρ_{xx} contour plot as a function of V_{BG} and B. The red (black) lines are the calculated position of $\nu = \pm 0, 4, 8, 12, \ldots$ of the top (bottom) layer. The layer filling factors (ν_T, ν_B) are indicated for each QHS.

up to a factor $4(e/h) = 9.67 \times 10^{10}$ cm^{-2} T^{-1}. Figure 3(c) summarizes the layer and total densities as a function of V_{BG}. We attribute the higher (lower) density to the bottom (top) layer, as it lies closer (farther) with respect to the back gate. Both layer densities go to zero at $V_D = 68$ V.

To understand the top (n_T) and bottom (n_B) layer density dependence on V_{BG} in twisted bilayer graphene, we employ a model used to calculate the layer densities in independently contacted graphene double layers separated by a dielectric.[23] The applied V_{BG} is distributed partly across the SiO$_2$ dielectric and partly on the Fermi energy of the bottom layer:

$$e(V_{BG} - V_D) = e^2(n_T + n_B)/C_{BG} + E_F(n_B). \quad (1)$$

Here $E_F(n) = \text{sgn}(n)\hbar v_F \sqrt{\pi |n|}$ is the Fermi energy relative to the charge neutrality point in monolayer graphene at a carrier density n, sgn represents the sign function, and $v_F = 1.1 \times 10^8$ cm s^{-1} is the Fermi velocity in monolayer graphene. Similarly, the bottom layer Fermi energy is the sum of the electrostatic potential difference between the layers and the Fermi energy of the top layer:

$$E_F(n_B) = e^2 n_T/C_{int} + E_F(n_T), \quad (2)$$

where C_{int} is the interlayer capacitance. Using Eqs. (1) and (2) and C_{int} as a fitting parameter, we calculate n_T and n_B as a function of V_{BG}. An excellent fit to the experimental

data is obtained for $C_{int} = 6.9$ μF cm^{-2} [solid lines in Fig. 3(c)]. Remarkably, this value is in good agreement with the interlayer capacitance expected theoretically for a Bernal stacked bilayer,[24] suggesting that the separation of the two layers in twisted bilayer graphene is close to that of a Bernal stacked bilayer. Two previous experimental studies[25,26] which examined electron transport in twisted bilayer graphene consisting of two exfoliated graphene mono-layers reported C_{int} values of 0.6 μF cm^{-2} (Ref. 25) and 6.8 μF cm^{-2}.[26]

Figure 4 shows the ρ_{xx} contour plot as a function of V_{BG} and B probed in the twisted bilayer sample of Fig. 3. The charge neutrality (Dirac) point is reached at a back-gate bias $V_D = 68$ V. The data show a QHS pattern which stems from the QHS superposition of the two decoupled monolayers. To map the position of the observed QHSs, we use Eqs. (1) and (2) to calculate the layers densities as a function of V_{BG} and B, with the only difference that the Fermi energy depends on both density and magnetic field as $E_F = E_N$, where $E_N = \text{sgn}(N)v_F\sqrt{2e\hbar B|N|}$ is the energy of the Nth LL in monolayer graphene, and $N = \text{Int}[nh/4eB]$ is the LL index; Int is the nearest integer function. Using $C_{int} = 6.9$ μF cm^{-2} extracted from Fig. 3 data analysis, we calculate n_B and n_T at fixed B and V_{BG} values, which are then converted into layer filling factors $\nu_{T,B} = n_{T,B}h/eB$. The black (red) lines in Fig. 4 represent the calculated position of half-filled LLs, i.e., $\nu_{B,T} = \pm 0, 4, 8, 12, \ldots$ for the bottom (top) layer. The ρ_{xx} maxima are in excellent agreement with the calculations, quantitatively confirming that the QHS sequence of twisted bilayer graphene is a superposition of the QHSs of the two graphene monolayers.

In summary, using a combination of Raman spectroscopy and magnetotransport measurements we established that CVD-grown bilayer graphene on Cu consists of a mixture of Bernal stacked and twisted monolayer domains. The Bernal stacked domains show QHSs at filling factors $\nu = 4, 8, 12$, in agreement with data in exfoliated bilayer graphene. The twisted bilayer graphene domains display a superposition of the individual QHSs of two graphene monolayers, which allows us to extract the layer densities and interlayer capacitance. The layer stacking determined from magnetotransport data correlates with the FWHM of the Raman 2D band.

---

*etutuc@mail.utexas.edu

[1] T. Ohta, A. Bostwick, T. Seyller, K. Horn, and E. Rotenberg, Science **313**, 951 (2006).

[2] E. V. Castro, K. S. Novoselov, S. V. Morozov, N. M. R. Peres, J. M. B. Lopes dos Santos, J. Nilsson, F. Guinea, A. K. Geim, and A. H. Castro Neto, Phys. Rev. Lett. **99**, 216802 (2007).

[3] J. B. Oostinga, H. B. Heersche, X. Liu, A. F. Morpurgo, and L. M. K. Vandersypen, Nat. Mater. **7**, 151 (2007).

[4] Y. Zhang et al., Nature (London) **459**, 820 (2009).

[5] C. Riedl, C. Coletti, T. Iwasaki, A. A. Zakharov, and U. Starke, Phys. Rev. Lett. **103**, 246804 (2009).

[6] K. Lee, S. Kim, M. S. Points, T. E. Beechem, T. Ohta, and E. Tutuc, Nano Lett. **11**, 3624 (2011).

[7] J. Hicks et al., Phys. Rev. B **83**, 205403 (2011).

[8] S. Lee, K. Lee, and Z. Zhong, Nano Lett. **10**, 4702 (2010).

[9] K. Yan, H. Peng, Y. Zhou, H. Li, and Z. Liu, Nano Lett. **11**, 1106 (2011).

[10]Z. Yan *et al*., ACS Nano **5**, 8187 (2011).

[11]Z. Luo *et al*., Adv. Funct. Mater. **21**, 911 (2011).

[12]A. C. Ferrari *et al*., Phys. Rev. Lett. **97**, 187401 (2006).

[13]C. Casiraghi, S. Pisana, K. S. Novoselov, A. K. Geim, and A. C. Ferrari, Appl. Phys. Lett. **91**, 233108 (2007).

[14]A. C. Ferrari, Solid State Commun. **143**, 47 (2007).

[15]L. M. Malard, M. A. Pimenta, G. Dresselhaus, and M. S. Dresselhaus, Phys. Rep. **473**, 51 (2009).

[16]Y. Hao *et al*., Small **6**, 195 (2010).

[17]S. Adam and S. Das Sarma, Phys. Rev. B **77**, 115436 (2008).

[18]E. McCann and V. I. Fal'ko, Phys. Rev. Lett. **96**, 086805 (2006).

[19]K. S. Novoselov *et al*., Nat. Phys. **2**, 177 (2006).

[20]J. M. Pereira Jr., F. M. Peeters, and P. Vasilopoulos, Phys. Rev. B **76**, 115419 (2007).

[21]U. Zeitler, A. J. M. Giesbers, A. McCollam, E. V. Kurganova, H. J. van Elferen, and J. C. Maan, J. Low Temp. Phys. **159**, 238 (2010).

[22]E. V. Kurganova, A. J. M. Giesbers, R. V. Gorbachev, A. K. Geim, K. S. Novoselov, J. C. Maan, and U. Zeitler, Solid State Commun. **150**, 2209 (2010).

[23]S. Kim, I. Jo, J. Nah, Z. Yao, S. K. Banerjee, and E. Tutuc, Phys. Rev. B **83**, 161401 (2011).

[24]H. Min, B. Sahu, S. K. Banerjee, and A. H. MacDonald, Phys. Rev. B **75**, 155115 (2007).

[25]H. Schmidt, T. Lüdtke, P. Barthold, E. McCann, V. I. Fal'ko, and R. J. Haug, Appl. Phys. Lett. **93**, 172108 (2008).

[26]J. D. Sanchez-Yamagishi, T. Taychatanapat, K. Watanabe, T. Taniguchi, A. Yacoby, and P. Jarillo-Herrero, Phys. Rev. Lett. **108**, 076601 (2012).